A New Approach to Lightweight Radar Altimeters

NADAV LEVANON, MEMBER, IEEE, FERREL G. STREMLER, MEMBER, IEEE, AND VERNER E. SUOMI

Abstract—Test results and key principles are given for a radar altimeter designed for meteorological balloons. The instrument, which weighs 160 g and consumes 0.7 W, will fill a gap in meteorological sensing using balloons—an area where pressure altitude was formerly the prevailing reference. The instrument is basically a delay-lock radar utilizing a superregenerative RF stage. Long-term absolute accuracy of ±10 m and short-term stability of better than 2 m rms were measured at altitudes of 20 km.

I. INTRODUCTION

LACK of convenient means of altitude measurement is partially responsible for the traditional reference, in meteorological sensing, to pressure altitude. The hydrostatic equation is usually—and not always justifiably—used to convert from the pressure scale to the altitude scale when the temperature is known. This traditional approach may change as a result of the recently developed and proven balloon-borne radar altimeter which is lightweight and low in cost and power consumption. This dispensable instrument is especially attractive for long-term overwater balloon applications because its absolute accuracy considerably surpasses that of the conventional balloon-borne pressure sensor.

The radar altimeter described here is a key component in the forthcoming Tropical Wind, Energy Conversion, and Reference Level Experiment (TWERLE). This experiment involves 400 superpressure floating balloons to be launched in the southern hemisphere starting in July 1974 with the NIMBUS-F satellite as navigator and data collector. Each balloon instrumentation package measures temperature, pressure, and absolute altitude and transmits this information, together with identification, to the satellite. Doppler signal histories made in each satellite pass are used for balloon location. Several experimental tests of instrumentation and balloons to be used in this experiment have been completed successfully and some results are cited in this paper.

Several unconventional approaches make it possible to build this rather simple and inexpensive, yet very accurate, radar instrument. A key factor is the utilization of a superregenerative RF stage, serving as both the receiver and the transmitter. In addition to the simplification obtained by a single RF stage, there are also the inherent advantages of equal transmitting and receiving frequencies, and a logarithmic response with wide dynamic range.

Because only one stage operates at the high frequencies, the design of the radar altimeter utilizes commercially available low-power integrated circuits. This results in low cost as well as low average power consumption.
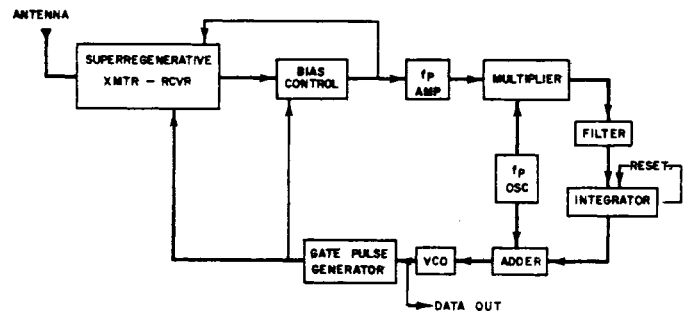
Fig. 1. Block diagram of the radar altimeter.

Considerable RF power saving is achieved by using the peak of the return signal rather than the leading edge. Additional RF power is saved by operating at the 400-MHz meteorological band rather than the 4.3-GHz altimeter band. This power saving comes from the dependence of the return signal on the second power of wavelength, as well as from the higher efficiency of solid-state devices at 400 MHz compared to 4.3 GHz. The low RF frequency is not necessarily accompanied by low antenna gain. The balloon application allows any antenna length, as long as the resulting radiation pattern can accommodate the expected pendulum motion of the balloon payload.

A delay-lock loop is used to provide a simple range tracking and measuring system, with the pulse repetition rate being (at lock) a measure of the altitude. Small perturbations added to the repetition rate are used to generate a range tracking error signal and have an effect equivalent to the split gate used in conventional tracking radars. The loop bandwidth controls an inherent averaging period. The RF pulses, with their repetition rate being a measure of altitude, can also serve, without any modification, as an altitude telemetry channel. This method of extracting the altitude information on the ground is sufficient for most ascending balloon applications. For floating balloons, the repetition rate is multiplexed on a telemetry channel for longer distance transmission.

II. PRINCIPLE OF OPERATION

A block diagram of the delay-lock [1] radar altimeter is shown in Fig. 1. The superregenerative RF stage [2] provides a receiving window followed by a transmitted pulse. When the pulse generator gates the RF power oscillator into an oscillatory mode, the presence of signal or noise sets the initial value of the growth of oscillations. The stronger the signal the shorter the delay before the oscillation amplitude reaches the saturation level. The high power oscillations are continued at the saturation level until cutoff by the termination of the gate (quench pulse).

The bias-control loop maintains a constant average width of the RF pulses, despite the tendency of the width to increase in the presence of signal, by adjusting the bias on the RF stage. The detected received signal is extracted from the
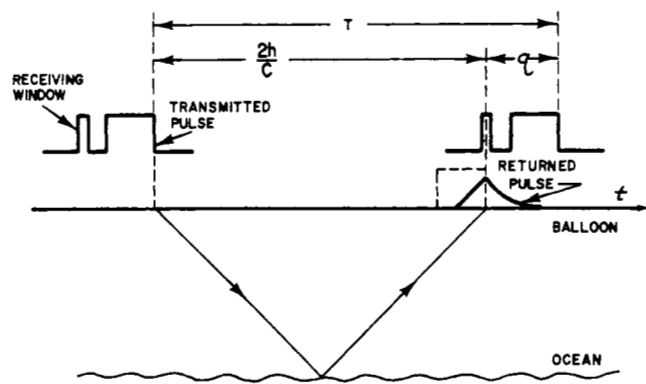
Fig. 2.   Timing diagram.

Fig. 3.   Typical waveforms of the quench, transmitted, and returned pulse.

bias circuit. As shown in [2], the superregenerative detector has a logarithmic response as long as it is allowed to reach saturation. This is the mode in which the altimeter operates.

The period of the quench pulses is controlled by the voltage-controlled oscillator (VCO) and is scanned from longer to shorter intervals. As the period coincides with the delay of the return, each receiving window detects the return from a preceding transmitted pulse. It should be noted that the scanning rate is relatively slow; hence an average return pulse is being reconstructed from many returns in a manner similar to the stroboscopic principle of a sampling oscilloscope. Some studies of the shape of the returned signal waveforms have been made over various terrains using this technique [3].

In addition, the signal controlling the repetition period of the altimeter is perturbed by a low-amplitude 200-Hz signal. This perturbation is detected on the slopes of the returned pulse, amplified, and then multiplied by the injected perturbation. This synchronous detection yields a signal proportional to the derivative of the returning pulse average waveform. The output of the multiplier is an error signal fed to the integrator whose output controls the VCO period. When the receiving window coincides with the peak of the return from a previous pulse, the derivative is zero; hence zero error signal is fed to the integrator and the loop locks. The sense of the error is such that the feedback loop keeps the receiving window aligned with the peak of the return in the locked condition. Dynamics of the loop are similar to those of the well-known phase-lock loop (PLL) [4].

The VCO repetition period at lock T is related to the altitude h by the following equation:

$$h = \frac{c}{2} (NT - \tau) \tag{1}$$

where c is the velocity of light and N is a subharmonic mode number which will be discussed in a later section on range ambiguity. Fig. 2 is a timing diagram for a first-mode case. This figure shows that the internal delay τ is measured between the receiving window and the end of the transmitted pulse, which, when this pulse returns, will be the position of the peak. To a first approximation, τ is equal to the width of the quench pulse, as could be explained with the help of Fig. 3. The position of the receiving window coincides with the leading edge of the quench pulse, because during this interval the RF stage crosses the line of oscillation state. The exponential buildup of oscillations occurs during the major part of τ. The signal power has to increase about 12 orders of
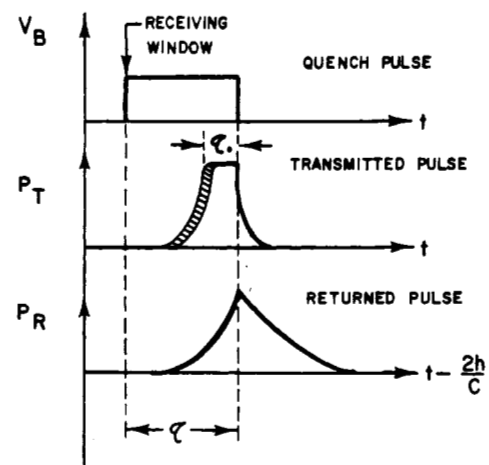
magnitude, and only the increase from one-tenth the saturation level will show on a linear scale. The fuzzy leading edge of the transmitted pulse is a result of each pulse building up from a different initial noise fluctuation.

In most cases, the shape of the returned pulse will be an imperfect integral of the transmitted pulse waveform [5]. This is a result of scattered reflections from the surface with pulse-length-limited illumination. The peak of the return will then coincide with the end of a rectangular transmitted pulse and therefore with the end of the quench pulse.

The setting of the width of the quench pulse and the assumption on the return pulse waveform are design parameters; hence τ is the only variable parameter in (1) and the main source of error. The limits on this error will be discussed in the following sections.

III. RETURN WAVEFORM AND POWER

The return signal waveform is the convolution of the transmitted pulse shape with the combination of the scattering coefficient, distance factor, and the antenna radiation pattern [5]. The scattering coefficient at near-vertical incidence (sometimes called the "quasi-specular" region) strongly affects the return waveform. If the terrain is perfectly smooth—e.g., salt flats—a true specular reflection will occur, i.e., the backscattering coefficient versus angle is a Dirac function at nadir, and the return signal will have the exact form of the transmitted pulse. If the terrain is a perfect scatterer, the scattering coefficient versus angle will be constant and the average return will be a perfect integral of the transmitted pulse as long as the antenna pattern and distance factor do not vary significantly.

Measured sea backscattering data [6] indicate typical linear variations of scattering coefficient versus incident angle of approximately 1 dB/1° for an average ocean, at 400 MHz, with incident angle between the vertical and 15° off the vertical. Backscatter data from ground terrain [7] are more variable and no single typical slope could be justified.

The conclusion from the preceding discussion is that at any fixed altitude the return waveform could change as a result of various backscattering conditions between the two extremes of 1) being a duplicate of the transmitted pulse or 2) being its integral. Furthermore, for any specific terrain, a change with altitude may also affect the return waveform. For example, at 13 500-m altitude a 100-ns pulse length oc-
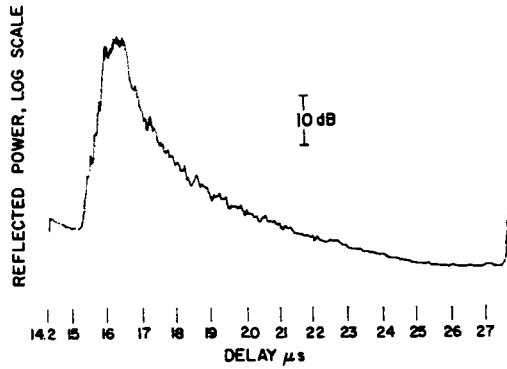
Fig. 4. Sea return recorded by an open-loop altimeter, with 500-ns transmitted pulse (Eilat Bay, Sept. 23, 1971).
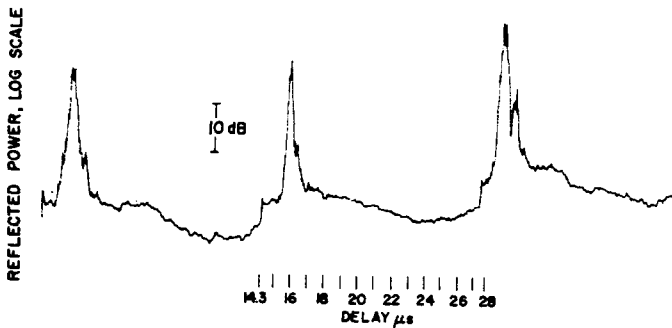

Fig. 5. Three consecutive land returns recorded by an open-loop altimeter, with 100-ns transmitted pulse (Negev Desert, Sept. 23, 1971).

cupies a 0.6° beamwidth angle. Over this limited angle the scattering coefficient could be assumed constant, and the return signal waveform will be closer to the integrated version of the transmitted pulse waveform. At 1500 m, the pulse length occupies a 6° angle which corresponds to approximately a 6-dB change in the scattering coefficient, tending to make the return waveform more like a duplicate of the transmitted pulse shape.

In summary, over extreme types of terrain and altitude ranges, the leading edge of the peak of the return signal waveform of a rectangular transmitted pulse could vary over at most a delay equal to the width of that pulse. For an RF pulse of 100-ns duration, this maximum delay is equal to a 15-m length, or ± 7.5 m.

Examples of return signal waveforms, as seen by the altimeter itself, are given in Figs. 4 and 5. They were obtained by opening the altimeter loop while allowing the period to continue the scan. In this open-loop mode, the recording of the bias voltage yields the average (by sampling) waveform of the return, as detected by the logarithmic response of the super-regenerative detector.

In Fig. 4, the waveform displayed is the return of a rectangular 500-ns transmitted pulse over the ocean (Eilat Bay, Israel), recorded from an approximate altitude of 2500-m. Fig. 5 includes three consecutive overland returns using a 100-ns pulse. The approximate spacings between successive returns are 1 min (the scanning period). The altitude is approximately 2300-m over the Negev Desert, Israel.

For typical values of the balloon-borne radar altimeter, such as a 3-dB antenna beamwidth of 50°, a transmitted pulse
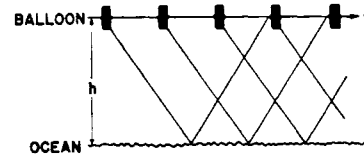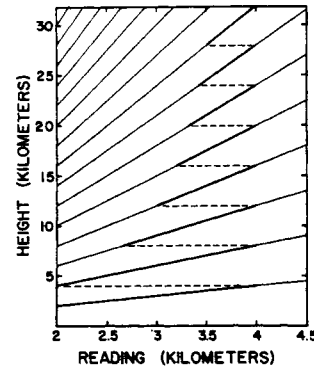

Fig. 6. Subharmonic operation.

Fig. 7. Ambiguity pattern for subharmonic operation.

length of 100 ns, and an altitude of 15 km, the illumination falls into the category known as "pulse-length-limited illumination, $\sigma°$ constant" [5]. For such a case, the received power at the peak of the return P_R is given as:

$$P_R = \frac{\lambda^2 G_0{}^2 \sigma_0{}° P_T c \tau_0}{4(4\pi)^2 h^3} \qquad (2)$$

where

λ the wavelength,
G_0 the antenna gain at nadir,
$\sigma_0{}°$ the average scattering coefficient at nadir,
P_T the power of the transmitted pulse,
c $= 299.8$ m/μs, the velocity of propagation,
τ_0 the width of the transmitted pulse,
h the altitude.

Typical values for the balloon-borne radar altimeter: $\lambda = 0.7$ m, $G_0 = 10$, $\sigma_0{}° = 1$, $P_T = 1$ W, $\tau_0 = 0.1$ μs, $h = 15$ km, will yield: $P_r = 6.9 \times 10^{-13}$ W, or -91.6 dBm.

IV. RANGE AMBIGUITY AND SUBHARMONIC OPERATION

The shortest possible pulse repetition period, as set by the VCO design, determines the minimum altitude of operation. There is no need, however, to set the upper limit equal to the maximum delay. The altimeter can operate in subharmonic modes in which one or more additional pulses are transmitted before the arrival of the return (Fig. 6). This subharmonic operation can occur starting at an altitude equal to twice the minimum altitude of operation. For continuous altitude coverage it is sufficient to set the maximum period of the VCO equal to twice its minimum period. An example of a possible mode-switching pattern during an ascent is given in Fig. 7, for a first-mode range of 2 to 4 km. The pattern in Fig. 7 assumes no loss of lock except at the end of the range for each mode; i.e., it is assumed that at any altitude the altimeter will operate at the lowest possible mode for that altitude. While being typical, this is not necessarily the case and a loss of lock might occur at
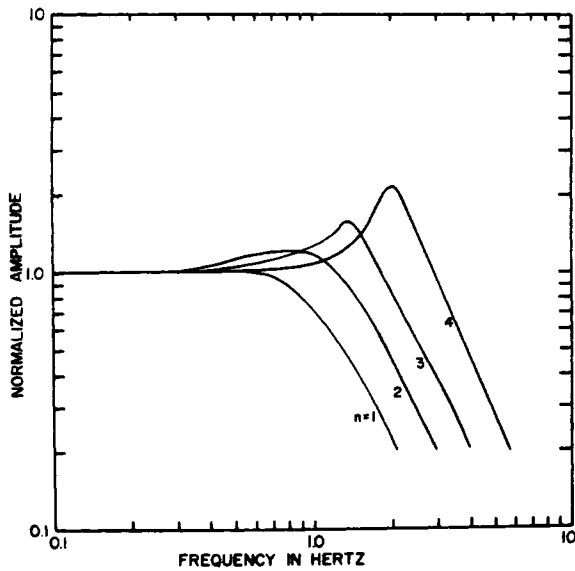
Fig. 8. Loop response for increasing mode numbers.

points other than the end points. In any case, the range ambiguity introduced is equal to at least the minimum altitude (2 km in our example). For meteorological applications, this can be resolved by pressure readings or by the history of the balloon ascent.

Subharmonic operation is desirable, to a certain extent, particularly at high altitudes because the pulse repetition frequency remains high, yielding more pulses per unit time. Therefore, there is a greater average transmitted power and a better signal-to-noise ratio [note the f_q term in (5)]. However, an upper limit on the subharmonic mode number is imposed by the problem of overlapping of return signals. The delay separation ΔT_N between the return of the Nth mode and the return of the $(N+1)$th mode is given by:

$$\Delta T_N = \left(\frac{2h}{c} + \tau\right)\frac{1}{N(N+1)} . \quad (3)$$

For the example of Fig. 7, and assuming $\tau = 0$, we calculate that at 20 km the separation between the fifth and sixth mode is 4.44 μs, while the separation between the ninth and the tenth mode is only 1.48 μs. The small latter separation means that the peak of the ninth return is superimposed on the trailing portion of the tenth return, and at a time delay of only 1.48 μs from the tenth peak. This may result in a limited leading edge for the ninth return and may be insufficient to maintain the lock.

A second problem in subharmonic operation is the dependence of the altimeter delay-lock loop bandwidth B_L on the mode number. The loop gain is linearly related to both the perturbation width and the VCO gain. However, these two are linearly related to the mode number and hence the loop gain is proportional to N^2. To a good approximation, the loop bandwidth is related to the square root of the loop gain [4], resulting in the relation:

$$B_L \propto N. \quad (4)$$

An experimental measurement of the loop response for various mode numbers is given in Fig. 8.

The preceding discussion assumes a VCO with a linear rela-

tion between voltage and period. If a conventional VCO (linear relation between voltage and frequency) is used, the above relationships are not linear and are dependent on which portion of the sweep is being used.

In summary, various tradeoffs exist which affect the choice of VCO range and mode numbers. Optimum performance could be achieved when a limited altitude range is expected. Some compromise in performance is required when the radar altimeter has to operate over a wide altitude range.

V. ALTITUDE MEASUREMENT ERRORS

Random errors in the altitude measurement arise from the deleterious effects of thermal noise in the range tracking loop and possible timing jitter in the receiver gate. Systematic errors may arise in the generation of the range error signal and residual errors in the range-tracking loop. Both types of error affect the value of τ in (1) and hence the range accuracy of the altimeter.

Range errors arising from timing jitter can be controlled by careful circuit design and are not a major source of error in the altimeter. To estimate the random range errors arising from thermal noise, it is convenient to describe the altimeter operation in terms of a split-gate range tracking radar, for which analyses already exist in the literature. Overall altimeter operation can be described as a narrow-gate sampler (the receiving window of the superregenerative stage), an averaging mechanism (the loop), and a split gate operating on the average detected pulse (the perturbation of the repetition rate).

Following an analysis by Barton and Ward [8], let us assume that the return pulse shape is Gaussian, the RF stage has a wide-band Gaussian bandpass, and that the perturbation waveform is a square wave (to correspond to a rectangular split gate). Under these conditions, the peak return signal power required to obtain a normalized (range) rms delay error σ_τ/τ_{3s} is [8]:[1]

$$P_i = \left(\frac{3}{2}\right)^2 \sqrt{\frac{\ln 2}{\pi}} \left(\frac{\sigma_\tau}{\tau_{3s}}\right)^{-2}\left(\frac{\tau_g}{\tau_{3s}}\right)^{-3} \frac{B_L N_0 F}{f_q \eta_f \tau_{3s}} \quad (5)$$

where

$$\eta_f = \frac{2B_h/B_s}{1 + (B_h/B_s)^2}$$

and

$$B_h > B_s$$

$$\tau_g < \tau_{3s}.$$

A list of the symbols used in (5) and typical values for an altimeter operating at 400 MHz is given in Table I. Using these numerical values, we get that the required peak return power should be -100.1 dBm to obtain a random rms range error of 1.5 m using an averaging period of 0.25 s. Comparison with the return power levels estimated in Section III shows that this is not an unreasonable demand for performance.

In practice, the return pulse shape is not Gaussian and the superregenerative stage does not have a Gaussian response, although these approximations are fairly good and do not

---

[1] Dynamic response of the range tracking loop can also cause interruption in tracking and is neglected in this result.

TABLE I

Symbol	Description	Typical value
B_h =	Rms width of superregenerative stage transfer function	33.2 MHz
B_s =	Rms width of signal voltage spectrum	8.3 MHz
B_L =	Overall altimeter loop bandwidth	2 Hz
F =	RF stage noise figure	8
f_q =	Pulse repetition frequency	30 kHz
N_o =	Density of uniform noise	5×10^{-21}w/Hz
τ_g =	Split-gate width	0.1μs
τ_{3s} =	Half-power width of signal	0.2μs
σ_τ =	Rms time-delay error	0.01μs(1.5m)

affect the result appreciably. The logarithmic detector characteristic accounts for a pulse integration loss on the order of 2 dB [9]. The perturbation waveform, as shown in the Appendix, is generally not a square wave and this accounts for some loss in tracking gain, on the order of 1–2 dB. These refinements are small, however, and (5) still provides a good estimate of the random range error arising from thermal noise.

An accurate determination of altitude using (1) requires an accurate knowledge of the parameter τ. Systematic errors arising from altimeter circuitry can either be measured or calibrated to some predetermined value. As noted in Section III, a limitation of this accuracy in actual operation is the lack of *a priori* knowledge of the return pulse shape. In extreme cases where the return signal waveform can vary between an integral and a replica of the transmitted pulse waveform, the absolute accuracy is simply limited by the width of the transmitted pulse. In applications limited to high altitudes, the return is more like an integral of the transmitted pulse shape. This better definition of the peak can result in a more accurate determination of altitude without further narrowing of the transmitted pulse waveform. Because the return pulse waveform is not in general symmetric near the peak, however, the choice of a perturbation waveform becomes important and range bias errors are introduced. This effect, as described in the Appendix, results in a range bias error toward higher altitude measurements. The magnitude of the error is on the order of one-fourth to one-half of the peak perturbation.

Another range bias error, which is oppositely directed to the above bias, arises from a residual sweeping voltage level in the delay-lock loop. To hasten acquisition, a small bias is applied to the integrator in the range-tracking loop to cause the loop to sweep toward higher repetition rates. At a preset level, the integrator resets and the cycle repeats until a signal return is present within the sweep range. To simplify the design, this small bias is not disabled at lock and results in a residual range bias error. This bias error is oppositely directed to that resulting from return pulse asymmetries.

Actual acquisition data measured on an altimeter attempting to lock on a simulated RF return are given in Fig. 9. The vertical axis is the delay (or repetition period) scale, the horizontal axis to the right is real time, and the horizontal axis to the left is the envelope of the return pulse. The parameter V is the sweeping rate. Fig. 9 demonstrates two phenomena: 1) the range bias error which increases with the sweeping rate and 2) an overshoot transient error which, as in the case of the largest sweeping rate V_4 shown, could prevent acquisition altogether.
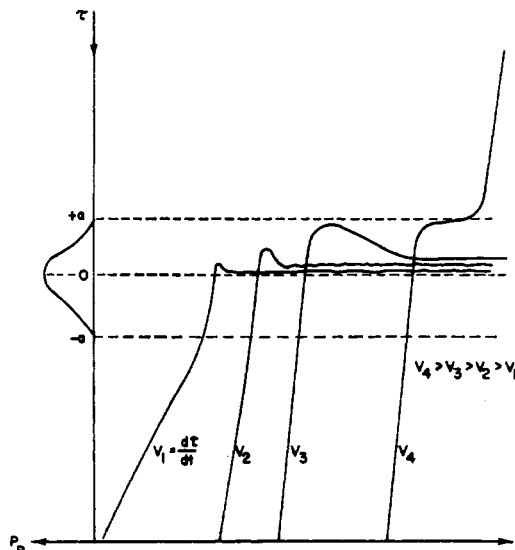

Fig. 9. Measured acquisition behavior with various sweeping rates.

The acquisition behavior of the sweeping (scanning) altimeter loop is similar to that of a second-order PLL following a frequency step. For any loop bandwidth one could define a "pull-out sweeping rate" which will prevent acquisition. The relation between the sweeping rate and the lower limit on loop bandwidth is more complicated than for the PLL, however, as a result of the dependence on the return waveform. Hence the design was based more on simulation results.

VI. TEST SYSTEM, DATA RECEPTION, AND SPECIFICATIONS

As with all the instruments on a balloon payload, the radar altimeter is normally tested on the site prior to launching. Because it is only one of several instruments, these tests must be kept simple and very straightforward. A simple passive test instrument has been developed which, together with a counter, yields both sensitivity and accuracy information. This test instrument includes only a variable attenuator and an electroacoustic delay line. The round-trip delay of the line is designed to be less than the altimeter scanning range so that the altimeter can lock on at least two consecutive multiples of the line delay. Measurements of the two periods of the altimeter when locking at the two consecutive delay-line multiples yield both the exact delay of the line, and the internal delay of the altimeter τ. The only drawback is the fact that the delay-line return is specular and a correcting factor has to be applied to the readings.

The variable attenuator supplements the delay-line insertion loss to simulate the path loss. The equivalent of one delay-line round-trip insertion loss has to be subtracted to cause altimeter locking on a higher delay multiple. Hence the recording of the required external attenuation to cause a loss of lock, at the two consecutive delay-line multiples, yields both the round-trip insertion loss of the delay line and the permissible round-trip attenuation for the altimeter.

During the balloon ascent, and usually for about 1 h at ceiling, it is possible to receive the altimeter RF pulses directly at the launching site. In addition to a receiver and counter, it is necessary to use a PLL on the video pulse train out of the receiver to narrow the video bandwidth while tracking the altimeter repetition frequency. This minimizes false counts and produces a very reliable measurement.
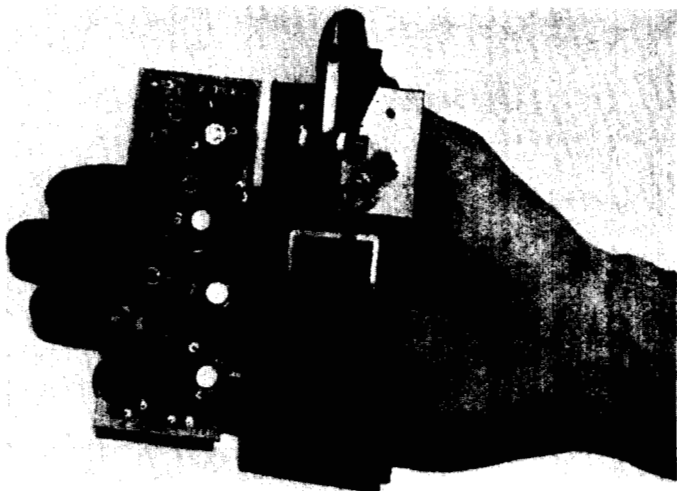
Fig. 10.   The radar altimeter electronics.

TABLE II

RF Frequency	415 MHz
Repetition Rate	27 - 40 KHz (25-37 µs)
Scanning Period	15 s
Internal Delay, τ	1.35 µs
RF Pulse Width	100 ns
RF Pulse Peak Power	1 W
Perturbation Width	0.1 µs @ delay of 100 µs
Power Input	+12v ±10%, 30 mA
	-12v ±10%, 30 mA
Operating Temperature	-55°C to +55°C (bare circuitry)
Weight (including antenna)	less than 160g
Accuracy	± 10 meters, ± 0.05%
Range (3rd mode)	11 - 16.5 km

For longer distance reception, the altimeter VCO frequency can be modulated on an available telemetry channel, such as a radiosonde. For very long distance reception, it is preferable to use a crystal-controlled counter on board to count the VCO frequency over a fixed interval and then send the digital code of the count. Because the altimeter has range ambiguities, some of the most significant bits in the count can be dropped before telemetering as long as the ambiguities introduced are no greater than the range ambiguities of the altimeter. In the TWERLE tests, a crystal-controlled signal gates the VCO output frequency with an accurate 2.56-s gate. Counting down is performed in a 14-stage counter, with the last 10 being read out. The counter is permitted to overflow to provide expanded resolution. This encoding scheme creates a 3.1-m resolution with 3.2-km ambiguity.

The radar altimeter is an all-solid-state device. The superregenerative stage utilizes a 400-MHz transistor in a microstrip circuit, shown on the right in Fig. 10. The other board includes the rest of the loop circuitry. The two boards are housed in a styrofoam box, and connected to a 5-element lightweight yagi antenna. Specifications of the radar altimeter for the TWERL experiment are listed in Table II.

VII. FLIGHT TEST RESULTS

The radar altimeter was tested in more than 40 flights, including aircraft flights, parachute drops, radiosonde balloon ascents, constant-level balloon flights, and tethered balloons.

Performance data are demonstrated in the figures of this section.

A. Absolute Accuracy

This parameter is the most difficult to measure in test flights. Most of our comparisons have been made during constant-level balloon flights between radar altimeter readings and ground-based radar measurements. In constant-level balloon flights, once the balloon arrives at ceiling, lack of timing synchronization between different altitude measurement sources should not contribute appreciable altitude errors. However, arrival at ceiling occurs after an ascent that lasts about an hour, during which time the balloon also drifts horizontally with the winds. By that time, tracking by the ground radar usually occurs at low elevation angles—an unfavorable condition for measurement of altitude. Results of one comparison appear in Fig. 11 in which a superpressure balloon carrying an altimeter and a pressure sensor was launched from Ascension Island and tracked by the NASA FPS-16 radar. Balloon telemetry yielded one altimeter reading every 3.5 min. The higher sampling rate of the ground radar data indicates balloon altitude fluctuations of about 50 m peak to peak and a 3–4-min period. With this departure from constant level, the timing errors force an average comparison. It should be noted that the ground radar locks on the large metal cap of the balloon; this cap is 100 ft above the altimeter, the last instrument in the payload. Similar comparisons were reported in [10] and [11].

B. Short-Term Accuracy

A graph of altimeter readings of an ascending radiosonde balloon over the Mediterranean recorded every 2 s is shown in Fig. 12 and demonstrates the short-term accuracy of the altimeter. The balloon burst near an altitude of 22 km, and altimeter readings at the beginning of the parachute descent are also included.

The rms value of the deviation from a smooth ascent (over the entire ascent record length of Fig. 12) was calculated using:

$$\sigma = \sqrt{\frac{1}{N} \sum_{i=1}^{N} (h_i - 2h_{i+1} + h_{i+2})^2}. \tag{6}$$

For the data shown in Fig. 12, this yields an rms error of 1.68 m. The counter gate period in this case was 1 s, which is also equal to the altimeter averaging period for this flight. It should be noted that part of these fluctuations is probably due to true variations in the balloon rate of ascent. A similar result was reported in [10] for the case of a radiosonde balloon ascent above Southern Wisconsin at a 10-km altitude.

Another demonstration of the short-term stability of the altimeter is given in Fig. 13. This is the second day in the life of the balloon AP/KW launched from Ascension Island on July 19, 1972. The data from the radar altimeter are plotted together with the data from an aneroid pressure sensor. The ratio of 50 m at 14.5 km versus 1 mbar at 143 mbars is very close to the ratio dictated by the hydrostatic equation (i.e., 44 m/mbar). The envelope around the data points was added to emphasize that the width of the short-term data spread is equal in both sensors, indicating true balloon movement. The sampling period of 3 to 4 min prevents one from resolving the balloon short-term altitude fluctuations. There is also a 1-min delay between the reading of the two sensors.
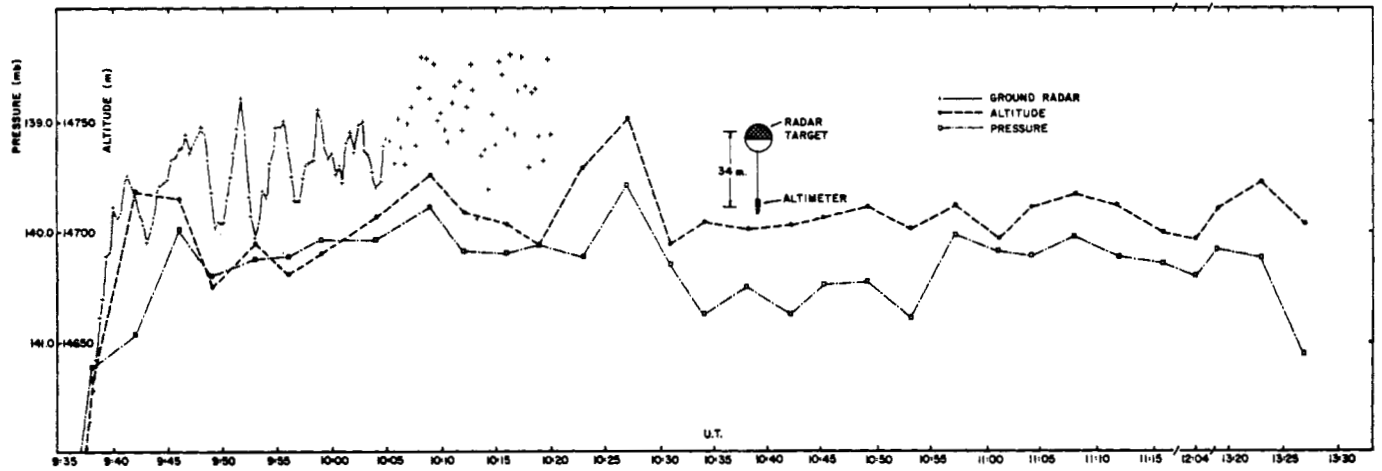
Fig. 11. Balloon-borne radar altimeter and pressure sensor data compared to ground radar reading. Balloon AC/SG, Ascension Island, July 10, 1972.
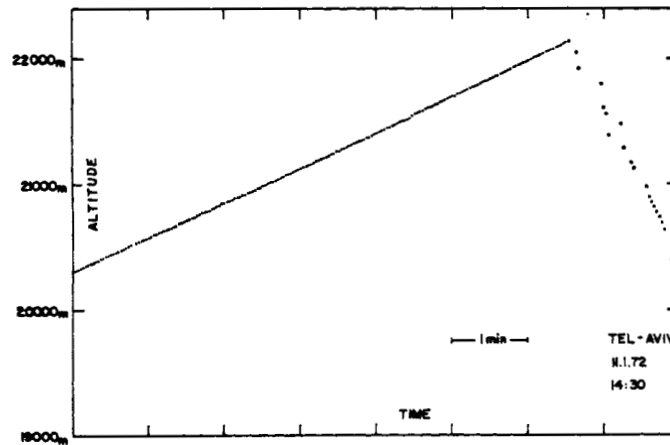
Fig. 12. Radar altimeter readings during radiosonde ascent, including balloon burst point and the parachute descent.
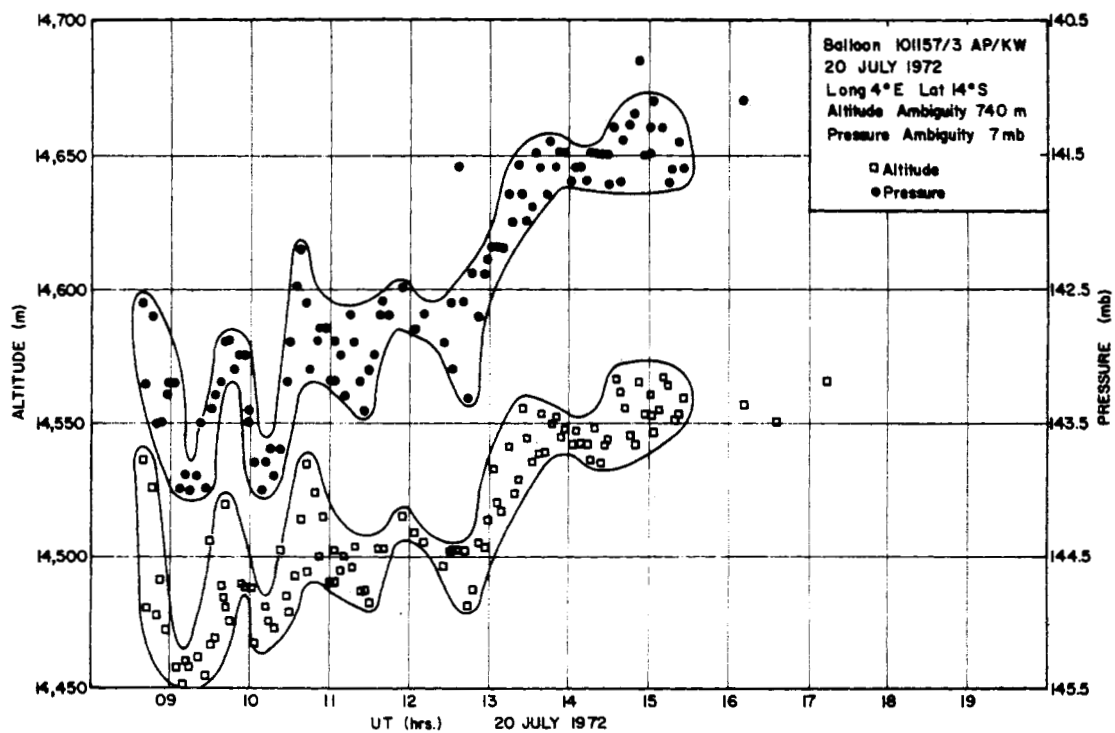
Fig. 13. Radar altimeter and pressure sensor readings, on the second day of a superpressure balloon flight, over the southern Atlantic.
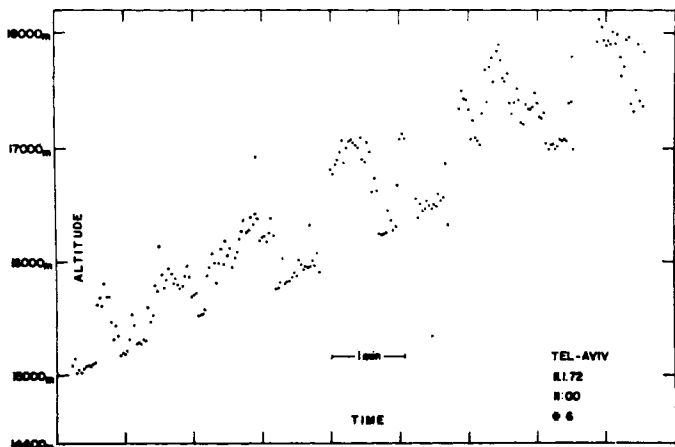
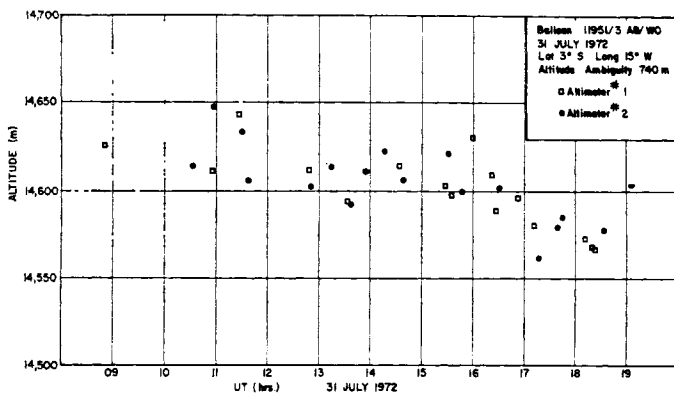Fig. 14. Radar altimeter readings during radiosonde ascent over mountain terrain.

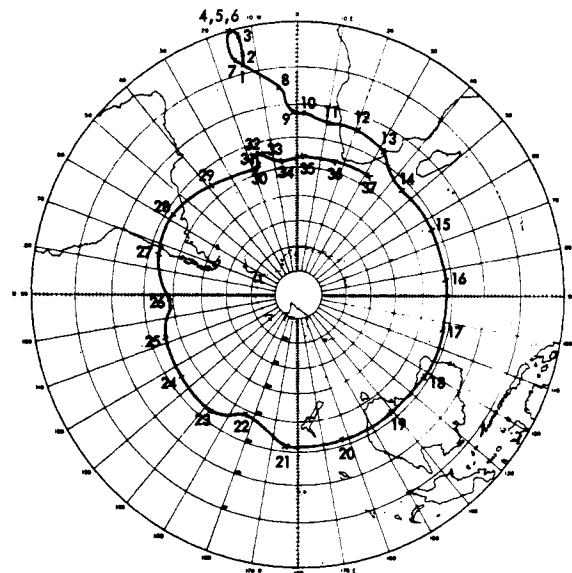Fig. 15. Comparison between two altimeters on the same superpressure balloon.

Fig. 16. The trajectory of superpressure balloon ATMOS-1. Numbers correspond to balloon days from Nov. 5, 1971. (Heinsheimer *et al.* [11].)

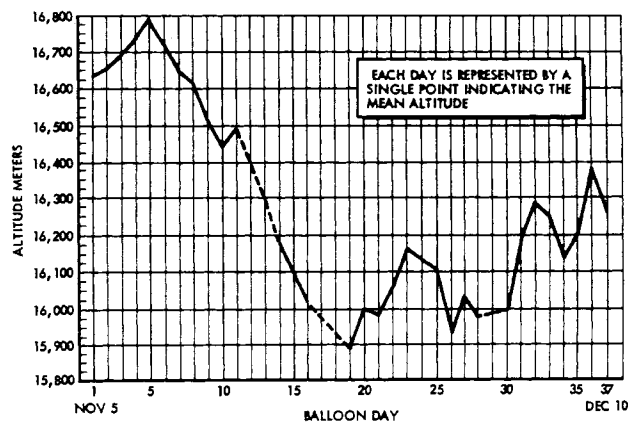Fig. 17. Altitude profile of ATMOS-1. (Heinsheimer *et al.* [11].)

C. Range

Although some problems were encountered in earlier prototypes, the present version of the altimeter has yet to fail measuring an altitude to which it was carried. The highest balloon-borne radar altimeter ascent was to 22 km (over ocean, Fig. 12), when the balloon burst before the altimeter reached its range limit. The highest balloon ascent over mountain terrain was 18 km (Fig. 14), and there again the balloon ceiling came before the altimeter ceiling. This was also the case in all of the superpressure balloon flights, including some recent flights at 18 km (80 mbars) in which altitude measurements were recorded both over the oceans and the continents.

D. Repeatability

A comparison between the reading of two altimeters was performed on a superpressure balloon AB/WO launched from Ascension Island on July 14, 1972. Two alternating altimeters were included in the payload, with a second channel used to identify which is the one on duty. Data taken on the 18th day of this balloon are shown in Fig. 15. Point-to-point comparison is again impossible because of rapid balloon altitude fluctuations. However, no significant altitude bias could be detected.

E. Reliability

The payload of a superpressure balloon suffers severe temperature cycling. A typical night temperature is −70°C, while a black painted payload may reach +30°C, inside temperature, during the day. The electronics in the altimeter is designed and tested for operating temperatures in the range of −55°C to +55°C. Of the twelve altimeters flown on board of superpressure balloons, in only one case the altimeter data became unintelligible before the balloon was lost. A summary of a typical balloon flight is given in Figs. 16 and 17, [11]. Fig. 16 includes the trajectory of the balloon during its life period of 37 days. Fig. 17 includes the balloon altitude profile. The sections of broken lines, in Fig. 17, indicate overland paths.

VIII. CONCLUSIONS

A means for an independent accurate measurement of geometric altitude is an important contribution to experimental studies of energy balance mechanisms in the atmosphere using balloons. The concept of using a very lightweight low-power inexpensive radar altimeter for these measurements has been shown to be both feasible and practical.

Several unconventional approaches were taken in the development of a radar altimeter to meet these objectives. They have yielded a low-weight radar altimeter design which permits operation from low-power solar panels without voltage regulation, without the need for active temperature compensation, and without the high-density structure which might prove hazardous to aircraft.
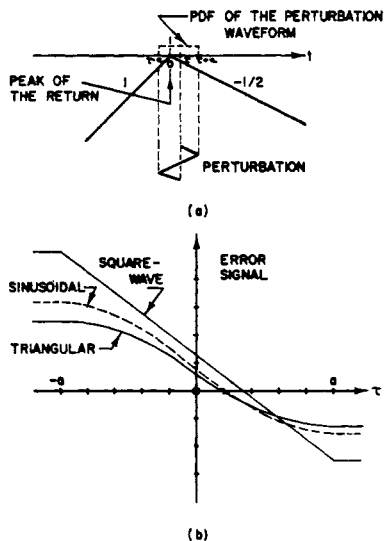
Fig. 18. Tracking error for three perturbation waveforms.

Limitations caused by range ambiguities can be resolved using pressure sensor data or ascent history. Long-term absolute accuracy of ± 10 m can be achieved up to high balloon altitudes. Present costs of 250 dollars per unit can be lowered substantially in large production quantities.

Results of test flights on superpressure floating balloons, ascending radiosonde balloons, and descending parachutes show that this type of radar altimeter is a very reliable way to measure geometric altitude accurately for meteorological experiments. The methods described here can be extended to other types of ranging problems in which the ambiguities are easily resolved.

APPENDIX

CHOICE OF RADAR ALTIMETER PERTURBATION WAFEFORMS

The altimeter attempts to lock to the peak of the average return. A perturbation is used to vary the positioning around the peak. This Appendix examines the effect of the perturbation waveform on the range bias error introduced in the measurement when the slopes in the return pulse are unequal.

As a simplified model of the average signal return, consider the one shown in Fig. 18(a). The method described here is also applicable to more complicated models but this one keeps the calculations simple. The return is positioned so that the peak is at $t=0$ for convenience. A timing perturbation is introduced and then synchronously detected. The result is integrated so that its mean value forms a range tracking error signal.

A convenient way to look at the effect of the perturbation waveform is to use its probability density function, a mapping by the average return pulse shape, and a calculation of its mean value after synchronous detection. Let $p(y)$ be the probability density function (pdf) of the perturbation waveform, and let the point τ indicate the displacement of the mean of the pdf from the true peak of the return. The synchronous detector introduces a "fold-over" at $y=\tau$, designated here by:

$$\text{sgn} (y) = \begin{cases} -1, & y < 0 \\ +1, & y > 0. \end{cases} \tag{7}$$

The mapping of the perturbation pdf from the delay axis to the amplitude axis is $g\{p(y)\}$. The detected mean value is then:

$$\eta(\tau) = \int_{-\infty}^{\infty} (y - \tau)g\{p(y)\} \text{ sgn } (y - \tau)dy. \tag{8}$$

As an example, let us restrict ourselves to symmetric waveforms with peak amplitude a and let the trailing edge of the return have one-half the (negative) slope as the leading edge. Results of the above integration for three perturbation waveforms are shown in Fig. 18(b).

From Fig. 18(b), several items of interest become apparent. A range bias error is introduced in the measurement. This error is in the direction of the less steep slope (i.e., trailing edge) of the return. As the pdf of the perturbation waveform is accentuated toward the lower amplitudes, the bias error decreases but the tracking gain also decreases. This loss in gain can be retrieved by changing other components in the loop.

Use of waveforms with nonsymmetric pdf's can result in zero range bias error if the asymmetries in the return pulse waveform were known and the pdf chosen in a complementary fashion. However, this *a priori* knowledge is not the usual case.

REFERENCES

[1] J. J. Spilker, Jr., and D. T. Magill, "The delay-lock discriminator—An optimum tracking device," *Proc. IRE*, vol. 49, pp. 1403–1416, Sept. 1961.
[2] G. O. Hall, "Superregenerative receivers," in *Microwave Receivers* (M.I.T. Rad. Lab. Ser.). New York: McGraw-Hill, 1948, ch. 20.
[3] N. Levanon, "Averaged pulse-shape measurements of radar sea return at near-vertical incidence," *IEEE Trans. Geosci. Electron.*, vol. GE-9, pp. 233–241, Oct. 1971.
[4] A. J. Viterbi, *Principles of Coherent Communication*. New York: McGraw-Hill, 1966, chs. 1–4.
[5] R. K. Moore and C. S. Williams, Jr., "Radar terrain return at near-vertical incidence," *Proc. IRE*, vol. 45, pp. 228–238, Feb. 1957.
[6] N. W. Guinard, J. T. Ransone, Jr., and J. C. Daley, "Variation of the NRCS of the sea with increasing roughness," *J. Geophys. Res.*, vol. 76, pp. 1525–1537, Feb. 1971.
[7] R. K. Moore, "Ground echo," in *Radar Handbook*, M. I. Skolnik, Ed. New York: McGraw-Hill, 1970, ch. 25.
[8] D. K. Barton and H. R. Ward, *Handbook of Radar Measurement*. Englewood Cliffs, N. J.: Prentice-Hall, 1969, ch. 3.
[9] V. G. Hansen, "Postdetection integration loss for logarithmic detectors," *IEEE Trans. Aerosp. Elec. Syst.* (Corresp.), vol. AES-8, pp. 386–388, May 1972.
[10] F. G. Stremler, N. Levanon, and V. E. Suomi, "A radio altimeter for balloon atmospheric sounding," in *AMS 2nd Symp. on Meteorological Observations and Instrumentation* (San Diego, Calif., Mar. 27–30, 1972), pp. 132–137.
[11] T. F. Heinsheimer, P. Trimm, and J. P. Pommereau, "The flight of ATMOS 1, an extended test of a balloon borne radar altimeter at the 100 mb level," presented at 7th AFCRL Scientific Balloon Symp., Portsmouth, N. H., Sept. 26, 1972.
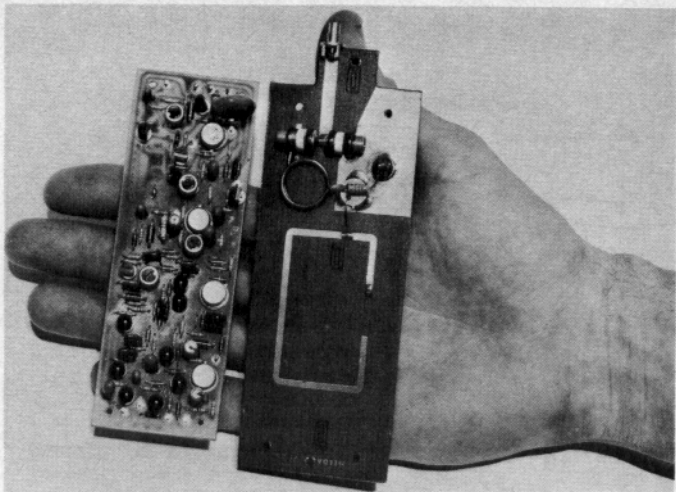
Fig. 10.   The radar altimeter electronics.